

Inversion of the Diffraction Pattern from an Inhomogeneously Strained Crystal using an Iterative Algorithm

A. A. Minkevich,^{1,*} M. Gailhanou,¹ J.-S. Micha,² B. Charlet,³ V. Chamard,¹ and O. Thomas¹

¹*TECSEN, UMR CNRS 6122 Université Paul Cézanne, 13397 Marseille Cedex 20, France*

²*UMR SPrAM 5819, CEA-Département de Recherche Fondamentale sur la Matière Condensée, F-38054 Grenoble Cedex 9, France*

³*LETI, CEA Grenoble, 38054 Grenoble Cedex 9, France*

(Dated: December 2, 2024)

The displacement field in highly non uniformly strained crystals is obtained by addition of constraints to an iterative phase retrieval algorithm. These constraints include direct space density uniformity and also constraints to the sign and derivatives of the different components of the displacement field. This algorithm is applied to an experimental reciprocal space map measured using high resolution X-ray diffraction from an array of silicon lines and the obtained component of the displacement field is in very good agreement with to the one calculated using a finite element model.

PACS numbers: 61.10.Nz; 62.20.-x; 42.30.Rx

The need to understand the physical properties of micro- and nano-crystals leads to a fast development of techniques aimed at probing the local structure. In addition, small objects have much higher yield stresses as compared to their bulk counterparts [1] and the vicinity of surfaces and interfaces implies strongly inhomogeneous stress fields. The experimental determination of the local strain remains, however, an open issue: electron microscopy has the required spatial resolution but suffers from the need for sample thinning down to electron transparency, which modifies the strain field [2]; High Resolution X-Ray Diffraction (HRXRD) is both strain sensitive and non-destructive but, as the phase of the scattered field is not experimentally accessible, the strain profile at the nanometer scale is only achieved through a model dependent approach [3, 4]. In this context, direct inversion based on x-ray diffraction is a rapidly progressing technique [5, 6, 7]. The possibility to directly determine the structure from a diffraction pattern alone was first mentioned by Sayre [8]. It is based on the "oversampling" conception, which allows to recover all Fourier components of an object as soon as the diffracted intensity pattern is sampled with a rate σ at least twice the highest frequency, namely the Nyquist frequency, which corresponds to the object size. The direct space electron density is retrieved with an iterative algorithm, first proposed by Gerchberg and Saxton [9], further developed by Fienup [10] and more recently by Elser [11]. It is based on back and forth fast Fourier Transforms (FT) together with a set of constraints in both direct and reciprocal spaces. This approach has been very successful in yielding the density distribution of noncrystalline materials [5] and crystals [12]. The strain distribution is more difficult to retrieve since an effective complex-valued density is used, where the amplitude is the density of the unstrained crystal and the phase is approximately given by the scalar product of the displacement \vec{u} with the reciprocal Bragg vector \vec{G}_{hkl} [13]. In this case, the conver-

gence of the standard algorithms is often problematic and has hindered so far the general applicability of inversion to the diffraction of strained objects. For some special shapes, the convergence may be achieved [14]. The first success concerning the case of a weakly strained nanocrystal has been recently obtained [6], but direct inversion of a diffraction pattern from a very non uniformly strained crystal remains an unsettled problem.

In this Letter, we present a modified iterative algorithm, where additional constraints on the spatial phase variations and on the crystal density uniformity are introduced. The algorithm is successfully tested on experimental data, where the displacement field retrieved from the x-ray diffraction pattern measured on a highly non uniformly strained crystal is in excellent agreement with the one calculated by finite element modeling based on continuum elasticity.

The Error Reduction (ER) [10] and the Hybrid Input-Output (HIO) [10, 15] iterative algorithms are standard inversion techniques used in so called lens-less x-ray microscopy. They are iteratively and cyclically used together with a set of direct and reciprocal spaces constraints. For a complex-valued density these constraints include the finite size of the support defining the object size and the measured intensity respectively. At each iteration k the difference between the calculated intensities and the experimental one is expressed as:

$$E_k^2 = \frac{\sum_{i=1}^N (|F_i^{calc}| - \sqrt{I_i^{meas}})^2}{\sum_{i=1}^N I_i^{meas}}, \quad (1)$$

where $|F_i^{calc}|$ is the magnitude of the calculated amplitude and I_i^{meas} is the measured intensity of pixel i in the Reciprocal Space Map (RSM). A lot of attempts to invert diffraction patterns obtained numerically from *a priori* defined sample shapes and displacement fields using this standard procedure were carried out and were unsuccessful. Each time the algorithm was started with a new set

of random phases, it converged to a different solution. Moreover it was found that there were a lot of solutions which corresponded to an error metric of $E_k^2 \approx 10^{-4}$. These solutions, however, exhibited very unrealistic features like jagged density and phase fields. It means that, in the case of an inhomogeneously strained crystal expressed as a complex-valued density, different combinations of amplitudes and phases in direct space can yield very similar FT amplitudes images. They correspond to local minima with very small error metric (1) causing the appearance of an ambiguity in the solutions. This is especially the case for experimental data where, because of the presence of noise, the difference between error metrics of correct and local minima solutions vanishes. It was found that one of the most important parameters responsible for this ambiguity is the maximum range of the displacement field derivatives with respect to each of the three directions of space. The probability to obtain different solutions with the same error metric increases when the range of these derivatives increases. Therefore without additional *a priori* knowledge the "phase problem" proved to be difficult to solve by this approach in the case of inhomogeneously strained objects. In this context, the introduction of some additional constraints to the direct space is mandatory. The cost of these constraints has, however, to remain small *i.e.* they should not require a fine pre-knowledge of the crystal to reconstruct. The approach presented in this Letter is restricted to the case of 2D plane strain systems and to chemically homogeneous crystals, although a generalization to 3D systems might be foreseen. In order to lift the above mentioned ambiguities, the following additional constraints in direct space were added:

I. The density must be uniform inside the support γ , except for a small region near the support edges $\tilde{\gamma}$, where it decreases in the external direction from the support (Fig. 1):

$$a_{k+1}(i) = \begin{cases} a'_k(i), & |a'_k(i) - c_k(i)| < \epsilon \\ a_k(i) + \beta(c_k(i) - a'_k(i)), & |a'_k(i) - c_k(i)| > \epsilon \end{cases} \quad i \in \tilde{\gamma} \quad (2)$$

$$c_k(i) = \begin{cases} 0, & i \notin \gamma \\ \frac{\sum_{\tilde{i} \in V_i} a_k(\tilde{i})}{N_{V_i}}, & i \in \gamma \setminus \tilde{\gamma} \\ a'_k(i), & i \in \tilde{\gamma} \end{cases}$$

with $a_k(i)$ - amplitude of pixel i of input (see [10]) at the k iteration, $a'_k(i)$ - amplitude of pixel i of output (see [10]) at the k iteration, the input $g_{k+1}(i) = a_{k+1}(i)e^{i\phi_{k+1}(i)}$ at the next iteration is taken from the output of the previous one by implementation of direct space constraints, β - parameter, which is taken in the [0.5, 1.0] interval, ϵ - parameter defining the threshold for applying the constraints (2) to each individual point i in the Direct Space Map (DSM), V_i - vicinity of point i , N_{V_i} - number of

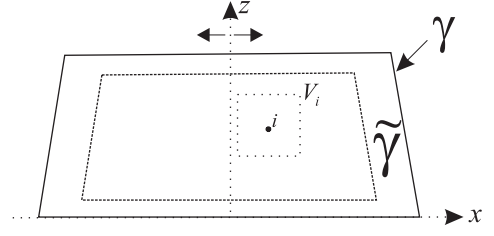


FIG. 1: Schematic sketch of the crystal cross section.

points in the V_i , $\tilde{\gamma}$ - narrow edge of support, the depth of this edge is defined by fittable parameters. The amplitude profile inside the edge $\tilde{\gamma}$ is constructed automatically by the iterative algorithm.

It was found that when the maximum range of the displacement field derivatives was small enough this constraint is sufficient and the phase field can be retrieved without ambiguity. When the amplitude of the derivatives variation increases, this constraint alone does not allow to find the solution anymore. For this reason a second constraint was added.

II. This second constraint is related to the maximum value that the components of the discrete displacement derivatives $\frac{\Delta_p u_j}{\Delta x_p}$ can take (Δx_p is a step along the p direction of the DSM defining the spatial resolution in this direction). This maximum value limits the possible phase difference between neighbouring points in the DSM:

$$|\phi_{k+1}(i) - \phi_{k+1}(i')| < G_{hkl} \Delta_p u_j^{max}, \quad (3)$$

where $\Delta_p u_j^{max}$ is a maximum difference in displacement component u_j between neighbouring points i and i' along p direction.

To make this constraint more efficient, it is necessary to define a minimum distance over which the displacement derivatives $\frac{\Delta_p u_j}{\Delta x_p}$ sign is constant. These distances depend on the particular properties of the sample, such as shape, symmetry, origin of strain, etc. and they can be fitted during an iterative process.

To implement these constraints in the iterative algorithm the maximum value of the displacement derivatives, namely the magnitudes $\Delta_p u_j^{max}$ have to be estimated. It was found that for the iterative algorithm a precise knowledge of the value of the maximum derivative is not very important. If the condition (3) is satisfied for most of the object volume, the constraint to the phases (3) should be switched off at the last cycles of the iterative algorithm. Alternatively instead of an estimation of the value of $\Delta_p u_j^{max}$, a trial-and-error procedure can be easily performed.

This constrained algorithm was used for the determination of the displacement field in Si lines on SiO₂/Si substrate. The Si lines were obtained by etching through a 160 nm thick Si₃N₄ mask a blanket 100 nm SOI (silicon

on insulator) film which lies on the top of a 200 nm BOX (Buried Oxide) layer (Fig. 2b). The direction of the lines is parallel to the [100] direction of the SOI crystal and to the [110] direction of the substrate crystal. The 2D high resolution diffraction pattern was measured on the french CRG beamline BM32 at ESRF around the 004 Bragg reflection (Fig. 2a) in the plane (x, z) normal to the sample surface and to the SOI lines ($x \parallel q_x \parallel \text{SOI [100]}$ direction, $z \parallel q_z \parallel \text{SOI [001]}$ direction, $y \parallel \text{SOI line}$). Here q_x and q_z are the components of $\vec{q} = \vec{k}_f - \vec{k}_i$, $|\vec{k}_f| = |\vec{k}_i| = \frac{2\pi}{\lambda}$, \vec{k}_i, \vec{k}_f - incident and diffracted wavevectors respectively, wavelength $\lambda = 1.54 \text{ \AA}$. This diffraction pattern contains only the information on the u_z component of the displacement field \vec{u} . The [001] directions of both crystals are misaligned by 0.4° . This small off-orientation enables the measurement of the diffraction pattern of SOI lines in the vicinity of \vec{G}_{004} Bragg vector without any overlap from the intensity scattered from the substrate. It is important to note on Fig. 2a the absence of periodic truncation rods related to the interference between lines in spite of an X-ray coherence length of around $6 \mu\text{m}$ in this direction, which is much larger than the $2 \mu\text{m}$ line period. This is due to important random phase shifts between lines, which might be related to very small (1 \AA range) - but comparable to the inverse of the scattering vector - ripples at the SiO_2 surface [16]. Since a lot of perfectly uniform lines are illuminated by the incidence beam with a coherence length much larger than the line width, the measured 2D diffraction pattern is equivalent to the diffraction pattern of a single SOI line. It is also important to note that only homogeneous strain can occur along y because of the line profile uniformity, and thus a 2D map is enough to extract the full inhomogeneous strain information compared to the general case where a 3D diffraction mapping is necessary. In order to be able to apply the iterative inversion algorithm to the measured intensity it is necessary to satisfy the oversampling condition $\sigma_{x,z} = \frac{M_{x,z}}{L_{x,z}} > 2$ in the DSM by choosing the appropriate step $\Delta q_{x,z} = \frac{2\pi}{M_{x,z}}$ in the RSM, where $M_{x,z}$ - size of the DSM and $L_{x,z}$ - expected size of object (support) in corresponding dimension x or z . It has been shown [17] that it is unnecessary to have an oversampling ratio $\sigma > 2$ in each dimension to retrieve 2D and 3D objects. However, practically for more reliable reconstructions it is better to have both $\sigma_{x,z} \gg 2$. In our experiment the oversampling ratio was chosen to be $\sigma_z \approx 7.8$ and is related to the number of measured points per thickness oscillation along q_z in the RSM. In the x direction the experimentally chosen step Δq_x corresponds to an oversampling ratio $\sigma_x \approx 6.3$. The steps $\Delta x \approx 7.9 \text{ nm}$, $\Delta z \approx 8.4 \text{ nm}$ in the DSM define the attainable resolution and relate to the size of the RSM. The size of the RSM is restricted by the area where the signal is above the background.

In addition to the direct space constraints discussed

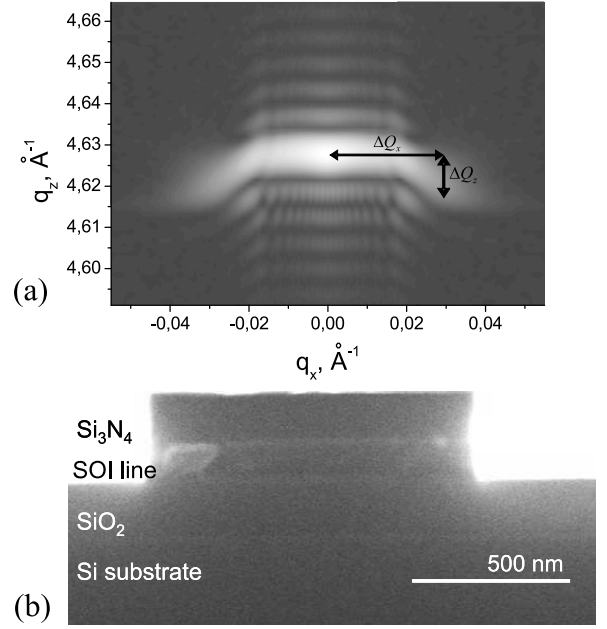


FIG. 2: (a) RSM measured near 004 reflection from Si lines on SiO_2/Si substrate. The intensity scale is logarithmic. (b) Scanning electron microscopy image of the corresponding sample.

in the first part of this Letter, the symmetry property of the displacement field with respect to the vertical axis z shown on Fig. 1 was used. An estimation of the maximum values of the displacement derivatives $\frac{\Delta_x u_z^{max}}{\Delta x}$, $\frac{\Delta_z u_z^{max}}{\Delta z}$ ($\Delta x, \Delta z$ are steps along x and z of the DSM respectively) was also carried out. The corresponding magnitude of the derivative of u_z along x is found from the distance ΔQ_x , shown on Fig. 2a, via the relation $\Delta Q_x = G_{004} \frac{\Delta_x u_z^{max}}{\Delta x}$. This value corresponds to a $\frac{3}{4}\pi$ maximum phase difference in the DSM between neighbouring points along x . Similarly the magnitude for the maximum displacement derivative u_z along z , $\frac{\Delta_z u_z^{max}}{\Delta z}$, is calculated from the distance ΔQ_z , shown on Fig. 2a, via the relation $\Delta Q_z = G_{004} \frac{\Delta_z u_z^{max}}{\Delta z}$. The validity of these estimations was checked at the end of the inversion.

The modified iterative algorithm was applied to the data in Fig. 2a, *i.e.* the direct space constraints were added to the iterative phase retrieval algorithm in addition to the standard support constraint. A good starting point for the shape was obtained from measurements on the scanning electron micrograph. The thickness oscillations along the z direction, which are clearly observed in the RSM, because of the small strain gradient in this direction, provided also a good estimation. The adaptive shrinkwrap procedure [18], which starts from a larger support and gradually removes from it the pixels whose amplitudes tend toward zero, does not work in our case. For this reason a support fitting procedure was developed, in order to gradually change the support

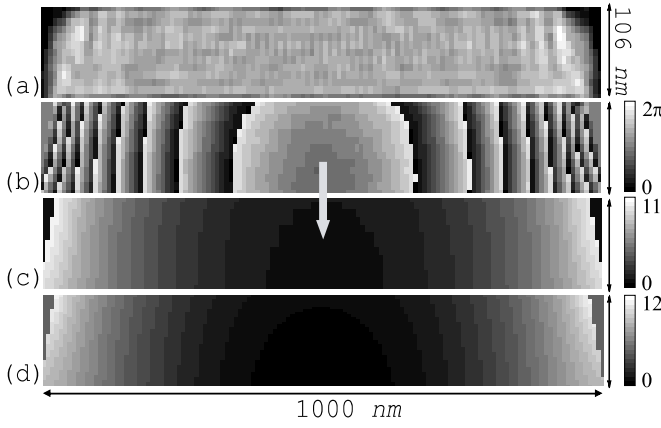


FIG. 3: The solution of the inverse problem: (a) amplitudes, (b) phases (in radians), (c) retrieved displacement field u_z (in Å), (d) displacement field u_z calculated by finite element modelling (in Å) [19].

area γ and the edge of the support $\tilde{\gamma}$ during the iterations. Generally one cycle of iterative algorithm included consecutively 50 iterations of ER, 50 iterations of HIO, 50 iterations of modified HIO (2) with phase constraints (3) and 50 iterations of modified HIO (only constraints to amplitudes (2)). If the support is very well defined (*i.e.* it corresponds to the exact shape of the object), the finding of solution takes about 4-8 cycles. Many trials of the algorithm were performed starting from random phases in RSM and each time converged to the solution with $E_k^2 \approx 10^{-4}$. With respect to the accuracy of the data all the solutions are the same, and one of them is plotted in Fig. 3. The shape determined using inversion (amplitudes) is in good agreement with the shape shown directly by the electron micrograph (Fig. 2b). The discontinuities in the retrieved phases map are related to the crossing of phases through 2π (2π corresponds to a displacement equal to $\frac{2\pi}{G_{004}}$). Some strain ϵ_{zz} along z is also found gradually appearing at the edges of the line, in the region, where the derivative $\frac{\partial u_z}{\partial x}$ becomes very high. This strain causes the appearance of the "moustache" shape intensity distribution in the RSM. There is also a small amount of homogeneous strain in the z direction, which was found from the difference in q between the Bragg maxima of SOI lines and Si substrate. Using the retrieved phases the displacement field was calculated (Fig. 3c). The maximum value of the displacement u_z is about 11Å.

The main advantage of this approach is its model independence as opposed to the case of, for example, finite

element calculations. Such calculations were also done for this sample, considering the residual stress in the Si_3N_4 top layer as the reason for the strain appearance in the line [19]. The displacement fields obtained by these two approaches are in very good agreement (Fig. 3c,d).

In conclusion, we have presented a modified iterative algorithm with additional direct space constraints. It is shown that the displacement field in a highly inhomogeneously strained crystal can be retrieved from its x-ray diffraction pattern alone. These results offer important perspective for local strain determination at the nanoscale.

The author A.A.M. is very grateful to S.Labat for discussions. The ESRF is acknowledged for beamtime allocation.

* Andrey.Minkevich@univ-cezanne.fr

- [1] E. Arzt, G. Dehm, P. Gumbsch, O. Kraft, and D. Weiss, Prog. Mat. Sci. **46**, 283 (2001).
- [2] M. M. J. Treacy, J. M. Gibson, and A. Howie, Phil. Mag. A **51**, 389 (1985).
- [3] T. Baumbach, D. Luebbert, and M. Gailhanou, J. Phys. D: Appl. Phys. **32**, A208 (1999).
- [4] Q. Shen and S. Kycia, Phys. Rev. B **55**, 15791 (1997).
- [5] J. Miao, P. Charalambous, J. Kirz, and D. Sayre, Nature **400**, 342 (1999).
- [6] M. A. Pfeifer, G. J. Williams, I. A. Vartanyants, R. Harder, and I. K. Robinson, Nature **442**, 63 (2006).
- [7] A. Y. Nikulin, Phys. Rev. B **57**, 11178 (1998).
- [8] D. Sayre, Acta Cryst. **5**, 843 (1952).
- [9] R. W. Gerchberg and W. O. Saxton, Optik (Stuttgart) **35**, 237 (1972).
- [10] J. R. Fienup, Appl. Opt. **21**, 2758 (1982).
- [11] V. Elser, J. Opt. Soc. Am. A **20**, 40 (2003).
- [12] G. J. Williams, M. A. Pfeifer, I. A. Vartanyants, and I. K. Robinson, Phys. Rev. B **73**, 094112 (2006).
- [13] S. Takagi, J. Phys. Soc. Jpn. **26**, 1239 (1969).
- [14] J. R. Fienup, J. Opt. Soc. Am. A **4**, 118 (1987).
- [15] R. P. Millane and W. J. Stroud, J. Opt. Soc. Am. A **14**, 568 (1997).
- [16] J. Härtwig, S. Köhler, W. Ludwig, H. Moriceau, M. Ohler, and E. Prieur, Cryst. Res. Technol. **37**, 705 (2002).
- [17] J. Miao, D. Sayre, and H. N. Chapman, J. Opt. Soc. Am. A **15**, 1662 (1998).
- [18] S. Marchesini, H. He, H. N. Chapman, S. P. Hau-Riege, A. Noy, M. R. Howells, U. Weierstall, and J. C. H. Spence, Phys. Rev. B **68**, 140101 (2003).
- [19] A. Loubens, Ph.D. thesis, Ecole Nationale des Mines de St-Etienne (2006).